Transcriptome landscape of a bacterial pathogen under plant immunity

Tatsuya Nobori[a], André C. Velásquez[b], Jingni Wu[a,1], Brian H. Kvitko[b], James M. Kremer[b,2], Yiming Wang[a], Sheng Yang He[b,c,3], and Kenichi Tsuda[a,3]

[a]Department of Plant Microbe Interactions, Max Planck Institute for Plant Breeding Research, 50829 Cologne, Germany; [b]Michigan State University-Department of Energy Plant Research Laboratory, Michigan State University, East Lansing, MI 48824; and [c]Howard Hughes Medical Institute, Michigan State University, East Lansing, MI 48824

Contributed by Sheng Yang He, February 2, 2018 (sent for review January 12, 2018; reviewed by Jeffery L. Dangl and Steven E. Lindow)

Plant pathogens can cause serious diseases that impact global agriculture. The plant innate immunity, when fully activated, can halt pathogen growth in plants. Despite extensive studies into the molecular and genetic bases of plant immunity against pathogens, the influence of plant immunity in global pathogen metabolism to restrict pathogen growth is poorly understood. Here, we developed RNA sequencing pipelines for analyzing bacterial transcriptomes *in planta* and determined high-resolution transcriptome patterns of the foliar bacterial pathogen *Pseudomonas syringae* in *Arabidopsis thaliana* with a total of 27 combinations of plant immunity mutants and bacterial strains. Bacterial transcriptomes were analyzed at 6 h post infection to capture early effects of plant immunity on bacterial processes and to avoid secondary effects caused by different bacterial population densities *in planta*. We identified specific "immune-responsive" bacterial genes and processes, including those that are activated in susceptible plants and suppressed by plant immune activation. Expression patterns of immune-responsive bacterial genes at the early time point were tightly linked to later bacterial growth levels in different host genotypes. Moreover, we found that a bacterial iron acquisition pathway is commonly suppressed by multiple plant immune-signaling pathways. Overexpression of a *P. syringae* sigma factor gene involved in iron regulation and other processes partially countered bacterial growth restriction during the plant immune response triggered by AvrRpt2. Collectively, this study defines the effects of plant immunity on the transcriptome of a bacterial pathogen and sheds light on the enigmatic mechanisms of bacterial growth inhibition during the plant immune response.

plant immunity | type III effector | microbiome | plant hormone | iron response

Photosynthate-rich plants provide an important growth niche for microbes including bacterial pathogens. In most cases, the plant immune system can effectively monitor microbial colonization and restrict the growth of a great majority of them (1). Excessive proliferation of evolved pathogenic microbes, however, can lead to plant diseases. Understanding how plant diseases occur and how the plant immune system effectively monitors and restricts pathogen infection represents one of the most important research areas in plant science.

Molecular genetic studies have revealed a repertoire of plant immune receptors and downstream immune-signaling components and their mode of actions within plant cells. As the first layer of the plant immune surveillance system, cell-surface pattern-recognition receptors recognize conserved molecular features of microbes such as bacterial flagellin and fungal cell wall components (chitin) to activate pattern-triggered immunity (PTI) (2, 3). To cause disease in plants, bacterial pathogens have evolved a battery of virulence molecules including type III effectors (T3Es) to subvert PTI (4). Plants, in turn, have evolved intracellular nucleotide-binding domain and leucine-rich repeat (NLR)-containing receptors, which recognize individual T3Es, as a second layer of the plant immune surveillance system, leading to effector-triggered immunity (ETI) (5). Although PTI and ETI receptors show distinctive cellular locations and biochemical properties, they share some downstream signaling components, such as signaling pathways mediated by the defense hormones salicylic acid (SA), jasmonate (JA), and ethylene (ET) (6). Despite extensive studies on the molecular, biochemical, and transcriptomic reprogramming within plant cells during immune activation, little is known about how plant immunity influences bacterial cellular processes and ultimately suppresses bacterial growth.

Previous studies have revealed bacterial processes that are important for their growth *in planta*. These include siderophores, exopolysaccharides, quorum sensing, multidrug resistance efflux pumps, plant hormones and their mimics, and toxins as well as T3Es secreted into the plant cell via the type III secretion system (T3SS) (4, 7–12). A number of T3Es suppress plant immune signaling as an important mechanism of bacterial virulence (13). T3Es have also been shown to manipulate plant intercellular (apoplastic) conditions to favor their proliferation. For instance, *Xanthomonas oryzae* uses T3Es, which function as transcriptional activators, to directly induce sugar-transporter genes, thereby

Significance

Plants have evolved a powerful innate immune system to defend against microbial pathogens. Despite extensive studies, how plant immunity ultimately inhibits bacterial pathogen growth is largely unknown, due to difficulties in profiling bacterial responses *in planta*. In this study, we established two methods for *in planta* bacterial transcriptome analysis using RNA sequencing. By analyzing 27 combinations of plant immunity mutants and *Pseudomonas syringae* strains, we succeeded in the identification of specific bacterial transcriptomic signatures that are influenced by plant immune activation. In addition, we found that overexpression of an immune-responsive *P. syringae* sigma factor gene involved in iron regulation could partially counter bacterial growth restriction during plant immunity. This study illuminates the enigmatic mechanisms of bacterial growth inhibition by plant immunity.

Author contributions: T.N., S.Y.H., and K.T. designed research; T.N., A.C.V., J.W., B.H.K., J.M.K., and Y.W. performed research; T.N. and K.T. analyzed data; and T.N., S.Y.H., and K.T. wrote the paper.

Reviewers: J.L.D., University of North Carolina; and S.E.L., University of California.

Conflict of interest statement: J.K. and J.L.D. are coauthors on a 2017 Perspective article.

Data Deposition: The RNA-sequencing data used in this study are deposited in the National Center for Biotechnology Information Gene Expression Omnibus database (accession no. GSE103442).

[1]Present addresses: National Key Laboratory of Plant Molecular Genetics, Shanghai Institute of Plant Physiology and Ecology, Chinese Academy of Sciences, 200032 Shanghai, China.

[2]Present address: AgBiome, Research Triangle Park, NC 27709.

[3]To whom correspondence may be addressed. Email: hes@msu.edu or tsuda@mpipz.mpg.de.

This article contains supporting information online at www.pnas.org/lookup/suppl/doi:10.1073/pnas.1800529115/-/DCSupplemental.

Published online March 12, 2018.

establishing sugar-rich apoplastic conditions (14). Some *Pseudomonas syringae* T3Es establish an aqueous apoplast in a humidity-dependent manner to promote bacterial proliferation (15).

It has been shown that PTI, if sufficiently activated, suppresses T3E translocation into plant cells, and this is associated with suppressed bacterial growth (16, 17). Also, a recent study showed that plants sequestrate sugars from the apoplast by activating sugar importers at the plasma membrane upon PTI activation, and this is associated with lowered T3E translocation and bacterial growth (18). These results suggest that suppressing T3E translocation is a way by which PTI inhibits bacterial growth. However, this mechanism does not fully explain the impact of PTI on bacterial growth restriction because PTI suppresses the growth of bacterial pathogens that do not possess T3SS (19). Similarly, ETI does not always affect T3E translocation even when ETI effectively suppresses bacterial growth (20). These results suggest the existence of immune targets other than T3SS. There is a need for a comprehensive and unbiased catalog of bacterial cellular changes influenced by plant immunity to gain insight into how PTI and ETI affect the biological processes of bacterial pathogens and inhibit their growth.

One approach to gain insight into bacterial cellular changes during plant immunity is *in planta* genome-wide transcriptome profiling. However, *in planta* bacterial transcriptome profiling is challenging due to low abundance of bacterial RNA compared with plant RNA, and it is particularly difficult to obtain a sufficient

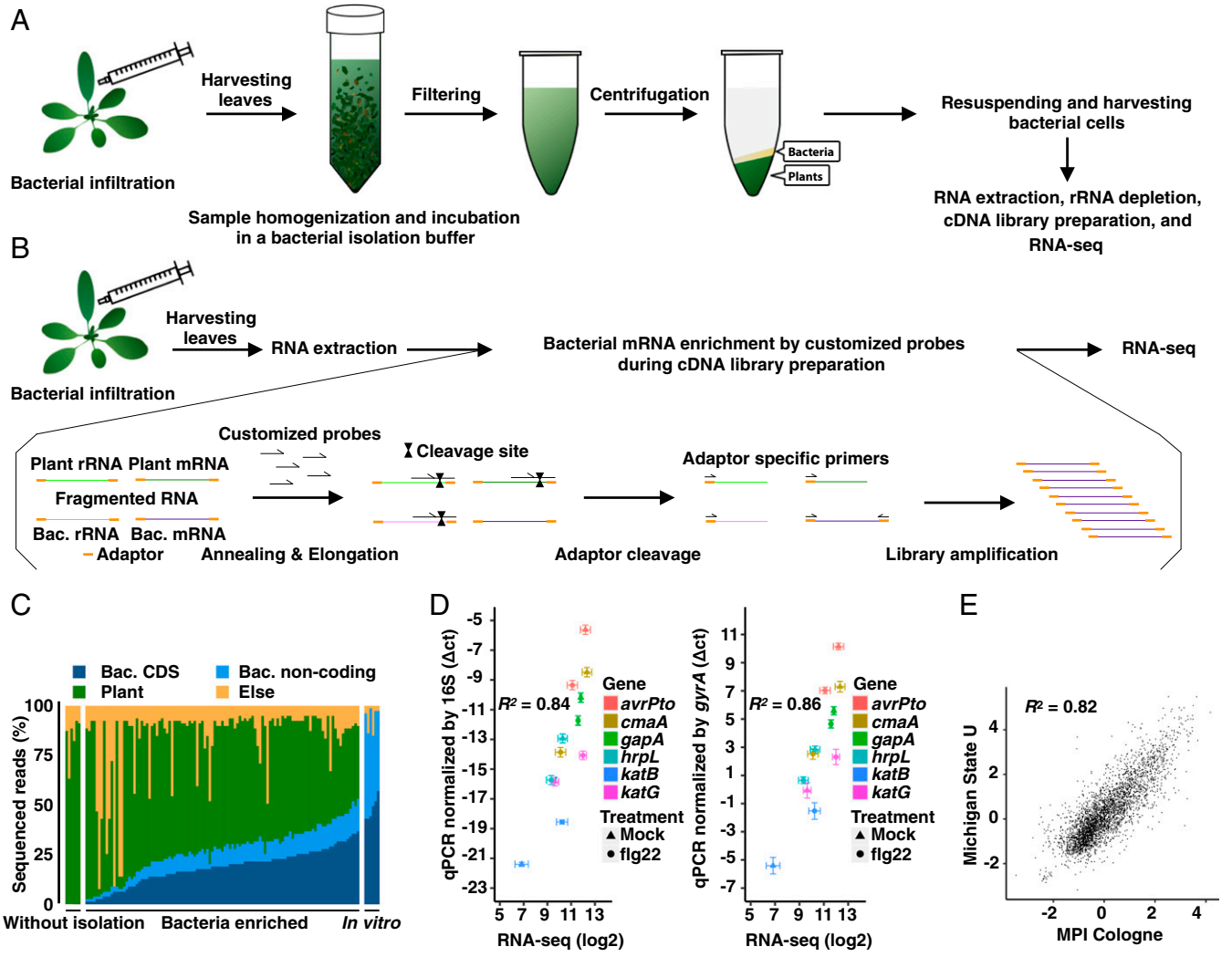

Fig. 1. Establishment of *in planta Pto* transcriptome analysis. (*A*) Workflow of *in planta* bacterial transcriptome analysis based on bacterial isolation (see *Materials and Methods* for further information). (*B*) Workflow of *in planta* bacterial transcriptome analysis based on selective depletion of plant-derived transcripts (see *Materials and Methods* for further information). (*C*) The ratio of sequenced reads mapped on the bacterial (Bac) CDS, bacterial noncoding sequence, *A. thaliana* (Plant) genome, and sequence reads that mapped to neither the *Pto* nor the *A. thaliana* genome (Else) in all samples, including samples without bacterial enrichment and in vitro samples. (*D*) Validation of RNA-seq data by RT-qPCR. Four-week-old *A. thaliana* leaves were pretreated with 1 μM flg22 or water (Mock) 1 d before infection with *Pto* (OD_{600} = 0.5) and were harvested at 6 hpi. The samples were split into two. One sample was subjected to direct RNA extraction followed by RT-qPCR analysis, and the other was subjected to bacterial enrichment followed by RNA-seq. RT-qPCR results were normalized with the *Pto* 16S or *gyrA* expression (mean ± SEM; $n = 4$ biological replicates from four independent experiments). RNA-seq data were processed as described in *Materials and Methods* (mean $\log_2$ count per million ± SEM; $n = 4$ biological replicates from four independent experiments). Pearson correlation coefficients (R^2) are shown. (*E*) Comparison of $\log_2$ fold changes in *Pto* gene expression in flg22-pretreated plants and mock-pretreated plants based on RNA-seq data independently obtained by two different approaches in two different laboratories: The method based on bacterial isolation from infected plants [Max Planck Institute Cologne (MPI), *x* axis] and on bacterial mRNA enrichment using customized oligonucleotides to remove abundant plant RNA without bacterial isolation [Michigan State University (U), *y* axis]. The Pearson correlation coefficient is shown. See *Materials and Methods* for detailed experimental procedures.

amount of bacterial RNA at an early stage of infection. Several previous studies profiled *in planta* bacterial transcriptomes by using microarrays and RNA sequencing (RNA-seq) (21–24). However, the impact of plant immunity on the entire bacterial transcriptome remains unknown.

Here, we established two RNA-seq methods for profiling the transcriptome of *P. syringae* in naive and immune-activated plant leaves at an early infection stage, 6 h post infection (hpi), when bacterial population density remained unchanged from 0 hpi. We reasoned that sampling at this time point could avoid secondary effects caused by different bacterial population densities *in planta*. Our methods greatly enriched bacterial transcripts from infected leaves, allowing us to uncover specific "immune-responsive" bacterial processes and genes that are altered during PTI and ETI. Using various combinations of *P. syringae* strains and immune-compromised plant genotypes, we showed that expression patterns of the immune-responsive genes at the early infection stage had a high predictive power for later bacterial growth at 48 hpi. Importantly, we found that overexpression of *pvdS*, a global iron regulator belonging to the immune-responsive gene sector, could partially counter bacterial growth inhibition during ETI triggered by AvrRpt2.

Results

Establishment of *in Planta* Bacterial Transcriptome Methods. To analyze the transcriptome of the model foliar bacterial pathogen *P. syringae* pv. *tomato* DC3000 (*Pto*) in *Arabidopsis thaliana*, we initially attempted RNA-seq using total RNA extracted from *A. thaliana* leaves infected by *Pto*. This approach failed to capture sufficient bacterial sequences, being masked by overwhelmingly abundant plant RNA sequences (Fig. S1 *A* and *B*). To overcome this limitation, we established a method in which bacterial cells are first isolated from infected leaves before RNA extraction (Fig. 1*A*). Infected leaves were harvested, coarsely crushed, and incubated in bacterial isolation buffer, which fixes and stabilizes bacterial RNA (Fig. S1*C*; see *Materials and Methods* for the establishment of a bacterial isolation buffer). After incubation, large plant debris was removed by filtering, and the flow-through was centrifuged to separate bacterial cells from plant tissues. Total RNA was extracted from the layer containing bacterial cells, followed by rRNA depletion of both plants and bacteria to enrich mRNA, library preparation, and RNA-seq. This method successfully enriched for bacterial sequences (Fig. 1*C* and Fig. S1 *A* and *B*), allowing us to profile high-quality *in planta* bacterial transcriptomes with as few as 10 million total RNA-seq reads using the Illumina HiSeq platform (Figs. S1 *C* and *D* and S2 *A*–*C*). RNA-seq results were highly reproducible among independent biological replicates and were sensitive enough to capture bacterial transcriptome differences between biologically distinct samples (Fig. S2 *B* and *C*). Gene-expression data obtained by this RNA-seq strategy strongly correlated with RT-qPCR measurements using total RNA extracted directly from *Pto*-infected leaves (Fig. 1*D*), indicating the accuracy of our RNA-seq data. To further assess the validity of our RNA-seq data, we compared our data with that from a more costly alternative approach in which bacterial mRNA was isolated directly from infected plants without prior bacterial separation from the plant tissue, but, instead, highly abundant plant mRNA as well as plant and bacterial rRNAs were removed by customized probes to enrich bacterial mRNA during cDNA library preparation (*Materials and Methods* and Fig. 1*B*). Note that these experiments were done completely independently in two laboratories with different growth conditions and pretreatments for plants, different preparations of bacterial inocula, and different kits for RNA extraction and cDNA library preparation (*Materials and Methods*). Strikingly, these two methods led to highly similar results (Fig. 1*E*), providing further proof of concept for both methods. Collectively, our methods enabled reliable profiling of *in planta* bacterial transcriptome with RNA-seq.

***Pto* Transcriptome Signatures Influenced by Plant Immune Activation.** We profiled *in planta Pto* transcriptomes under 27 conditions and in vitro *Pto* transcriptomes under five conditions using the method shown in Fig. 1*A* (114 samples in total), Fig. 2*A*, and Fig. S3; see Dataset S1 for the full sample list with the number of replicates. Four *Pto* strains were employed. The wild-type *Pto* strain has T3Es that effectively suppress plant immunity in *A. thaliana* wild-type Col-0, resulting in effector-triggered susceptibility (ETS). *Pto* strains that ectopically express a T3E, i.e., AvrRpt2 or AvrRps4 (hereafter *Pto* AvrRpt2 or *Pto* AvrRps4), trigger ETI dependent on the presence of cognate plant intracellular immune receptors, RPS2 or RPS4, respectively (25–27). The *Pto* D36E mutant lacks all 36 known *Pto* T3Es (28). In our conditions, bacterial proliferation was observed at 9 hpi, but not at 6 hpi (Fig. S4), in both ETS and ETI in WT Col-0 plants and in highly immune-compromised *dde2 ein2 pad4 sid2* mutant plants (29). Thus, we decided to profile the *in planta Pto* transcriptome at 6 hpi because bacterial population density affects bacterial gene expression patterns, e.g., through quorum sensing (30). All four *Pto* strains showed similar transcriptome patterns in nutrient-rich King's B bacterial growth medium; these patterns were distinct from that of *Pto* grown in T3E-inducible minimal medium (MM) (Fig. 2*B* and Fig. S5*A*) (31). As expected from the previous studies (32), genes related to the T3SS and T3Es were globally induced in MM compared with King's B medium (Fig. 2*C*). Gene ontology (GO) analysis revealed that genes related to the T3SS and coronatine biosynthesis (12) were induced in plants compared with King's B medium (Fig. 2*C* and Dataset S3), consistent with the crucial roles of T3SS and coronatine for *Pto* virulence (33, 34).

Pretreatment with a PTI elicitor derived from bacterial flagellin, flg22, triggers strong plant transcriptional reprogramming and resistance against bacterial pathogens (35). However, the impact of flg22 treatment on any bacterial transcriptome remains unknown. We found that pretreating plants with flg22 affected a substantial number of *Pto* genes and globally suppressed the *in planta*-activated bacterial processes (Fig. 2*C*). The transcriptome patterns of *Pto* D36E *in planta* resembled that of *Pto* in flg22-pretreated plants (Fig. 2 *B* and *C* and Fig. S5*A*). This supports the notion that effectorless *Pto* D36E lacks the ability to suppress PTI and that preactivation of PTI with flg22 can overcome effector-mediated immune suppression by wild-type *Pto*. Importantly, these results revealed that PTI suppresses not only bacterial virulence-associated mechanisms such as the T3SS and siderophore and coronatine biosynthesis but also fundamental housekeeping processes for organisms. For instance, genes related to translation (mostly ribosomal proteins) were induced in *Pto in planta* but were suppressed by PTI (Fig. 2*C*), implying that the bacterial protein synthesis activity may also be targeted by PTI.

During ETI triggered by AvrRpt2 or AvrRps4, several hundred genes (199 genes for AvrRpt2 and 317 genes for AvrRps4) were differentially expressed compared with ETS (*Pto* infection; Fig. 2*C*), although the effect was not as dramatic as for PTI (Fig. 2*B*). In particular, we found that ETI triggered by AvrRpt2 and AvrRps4 specifically led to down-regulation of genes associated with siderophore and coronatine biosynthesis (Fig. 2*C*). However, T3SS genes were not globally affected during ETI, in contrast to PTI-inducing conditions, suggesting that PTI and ETI share only a subset of *Pto* transcriptomic changes despite their overlapping downstream immune-signaling components and their common ability to inhibit bacterial growth *in planta*. In addition, within the genes differentially expressed among the different conditions, 658 genes were annotated as "hypothetical proteins" (Fig. S5*B*), suggesting that a substantial number of *Pto*

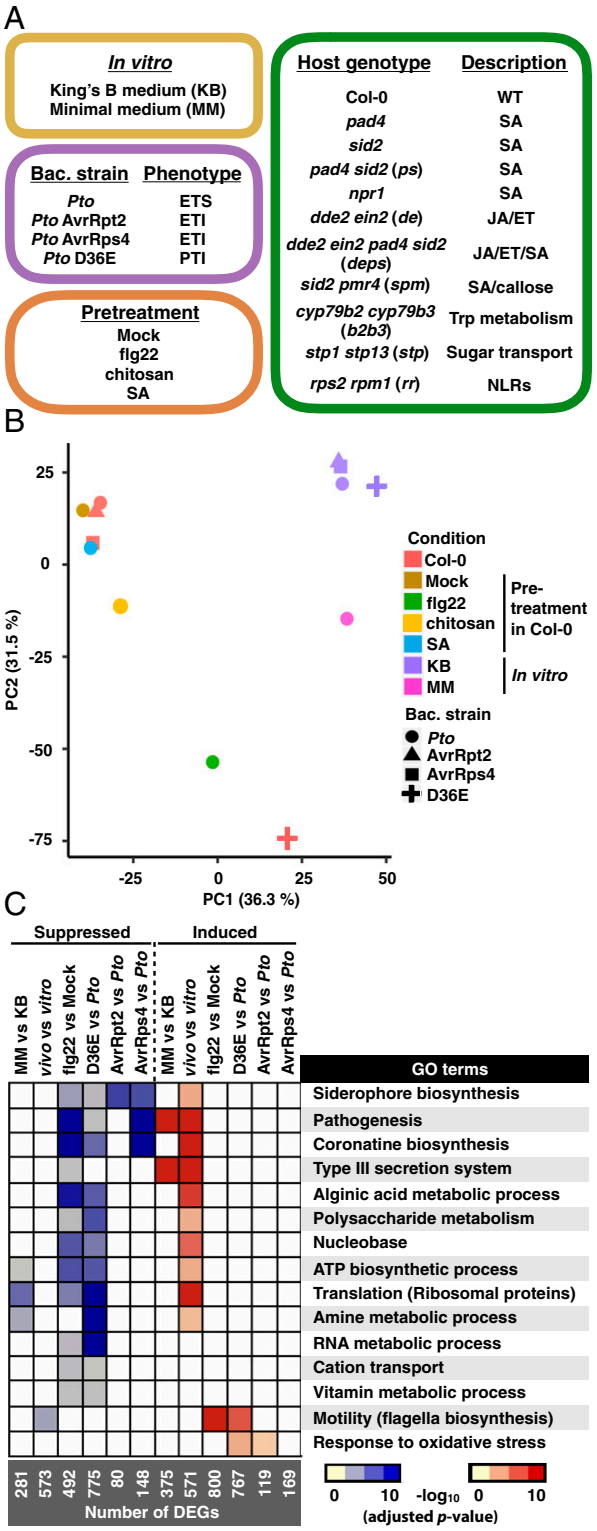

Fig. 2. Profiles of the *Pto* transcriptome under various conditions. (*A*) Plant genotypes, bacterial (bac.) strains, and conditions used in this study. For the full sample list, see Dataset S1. ET, ethylene; ETI, effector-triggered immunity; ETS, effector-triggered susceptibility; JA, jasmonic acid; NLRs, nucleotide-binding domain leucine-rich repeat proteins; PTI, pattern-triggered immunity; *Pto*, *Pseudomonas syringae* pv. *tomato* DC3000; SA, salicylic acid; Trp, tryptophan. (*B*) Principle component analysis of 3,344 genes detected in all samples. (*C*) Heatmap of $-\log_{10}$ *P* values (adjusted by the Benjamini–Hochberg method) of GO terms representing the DEGs in different comparisons. KB, *Pto* in King's B medium; MM, *Pto* in MM medium; *vitro*, *Pto* in King's B medium; *vivo*, *Pto* infection in Col-0. For the list of differentially expressed genes and complete enriched GO terms, see Datasets S2 and S3, respectively.

genes likely playing roles during the interaction with *A. thaliana* have yet to be characterized. Taken together, our data revealed previously unknown transcriptomic responses of *P. syringae* during the activation of two major forms of plant immunity, PTI and ETI.

***In Planta* Bacterial Transcriptome Patterns at an Early Time Point Are Tightly Linked to Later Bacterial Growth During Infection.** Plant signaling pathways mediated by defense hormones SA, JA, and ET contribute to bacterial growth suppression in a redundant manner (6). However, it is not known whether these hormone-signaling pathways affect the bacterial transcriptome similarly or differently. To address this question, we investigated transcriptome patterns of *Pto* or *Pto* AvrRpt2 in seven different *A. thaliana* mutants lacking one or more of these hormone defense pathways (Fig. 2*A*). Host genotype effects were observed more clearly for *Pto* AvrRpt2 infection than for *Pto* infection at 6 hpi; 321 genes of *Pto* AvrRpt2 were differentially expressed between Col-0 plants and at least one of the defense-signaling mutants, while only 26 genes of wild-type *Pto* were differentially expressed. We focused on the differentially expressed genes (DEGs) of *Pto* AvrRpt2 (Fig. 3*A*, *Left*; blue/yellow heatmap) for further analysis. Comparisons between Col-0 and the immune-compromised mutants revealed that the effects of distinct hormone pathways were qualitatively similar (Fig. 3*A*, *Center*; green/magenta heatmap). For example, the genes suppressed by the SA pathway were also suppressed by the JA/ET pathway. This implies that different immune pathways may converge on a common impact on the global gene expression of *Pto*. In addition, the expression patterns of the DEGs at 6 hpi, when bacterial population density remained unchanged compared with that observed at 0 hpi (Fig. S4), strongly correlated with bacterial growth at 48 hpi in different plant genotypes ($R^2 = 0.94$) (Fig. 3*B*), suggesting that bacterial transcriptome patterns at the early phase of infection could explain future bacterial growth.

CYP79B2 and *CYP79B3* encode enzymes required for tryptophan-derived defense secondary metabolites including camalexin and 4-hydroxyindole-3-carbonyl nitrile (36, 37). *STP1* and *STP13* encode sugar transporters, which were shown to sequester sugars from the extracellular space where foliar bacterial pathogens colonize (18). Previous studies showed that tryptophan-derived defense secondary metabolite production and sugar sequestration contribute to resistance against *Pto* (18, 38). In the present study, *Pto* and *Pto* AvrRpt2 transcriptomes in *cyp79b2 cyp79b3* and *stp1 stp13* mutants were similar to those in Col-0 (Fig. 3*A*).

The System of Bacterial Iron Acquisition Is Influenced by Plant Immunity. The host genotype-dependent DEGs in *Pto* AvrRpt2 could be separated into six clusters based on the expression patterns, which were then subjected to GO analysis (Fig. 3 *A* and *C* and Datasets S4 and S5). In cluster II, genes related to siderophore biosynthesis, which is known to be induced under iron-deficient conditions and to scavenge iron from the environment, were induced *in planta* and suppressed by both PTI and ETI (Fig. 3*C*). Because both PTI and ETI impact the expression of iron-related genes, we investigated the link between bacterial responses to iron and plant immunity. Of the 133 previously reported iron-responsive genes in in vitro-grown *Pto* (39), a significant number (69 genes) were differentially regulated by plant immunity (4.8-fold over-enriched; $P = 1.89e^{-37}$; hypergeometric test) (Fig. 4*A*; overlap between the red and green bars). More strikingly, of the 69 genes coregulated by iron and plant immunity, iron-repressive genes were almost exclusively suppressed by plant immunity, whereas iron-inducible genes

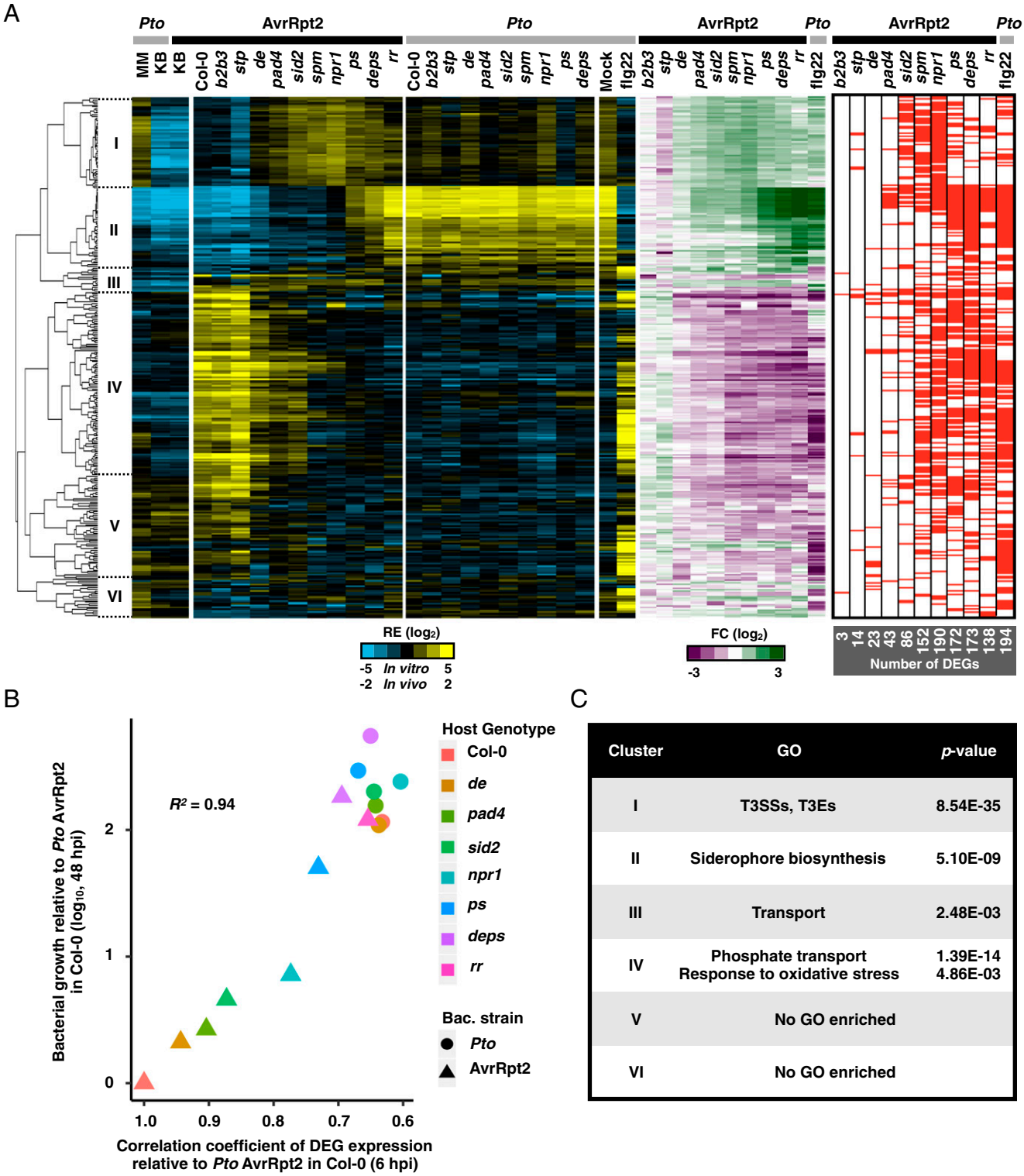

Fig. 3. Host genotype effects on bacterial transcriptome. (*A*, *Left*; blue/yellow heatmap) Hierarchical clustering of the relative expression (RE) of the DEGs in *Pto* AvrRpt2 based on the pairwise comparisons between Col-0 plants and the mutant plants (FDR < 0.01; $|\log_2$ fold change$| > 2$; represented by the red marks in the heatmap on the *Right*). (*Middle*; green/magenta heatmap) Fold changes in *Pto* AvrRpt2 gene expression in defense-mutant plants compared with those in Col-0 plants or fold changes in *Pto* in flg22-pretreated Col-0 plants compared with mock-pretreated Col-0 plants. *Pto* and *Pto* AvrRpt2 are represented by gray and black marks, respectively. See Dataset S4 for the list of DEGs. (*B*) The relationship between the expression pattern of the bacterial DEGs at 6 hpi and bacterial growth at 48 hpi. The Pearson correlation coefficient is shown ($R^2 = 0.94$). The genes of *Pto* AvrRpt2 identified as DEGs in at least one of the pairwise comparisons between Col-0 and mutant plants (FDR < 0.01; $|\log_2$ fold change$| > 2$) were used for the analysis. The *x* axis represents Pearson correlation coefficients of DEG expression patterns between each sample and *Pto* AvrRpt2 in Col-0 plants. The *y* axis represents increased bacterial growth levels in each sample compared with *Pto* AvrRpt2 in Col-0 plants at 48 hpi (29). (*C*) List of GO terms enriched in the clusters shown on the left of the dendrogram in *A*. For the full GO list, see Dataset S5. See Fig. 2*A* for the acronyms.

involved both immune-inducible and immune-repressive genes (Fig. 4*A*). Thus, plant immunity modulates a part of the bacterial iron responses.

***pvdS* and Its Regulatory Targets Are Commonly Suppressed by PTI and ETI.** We investigated the promoter region of iron-responsive genes for the binding motifs of Fur and PvdS, both of which are known to be involved in iron responses (Fig. 4*A*) (40). Fur is the primary regulator of iron homeostasis and, in the presence of iron, typically functions as a repressor of the downstream iron responses (40). PvdS, an extracytoplasmic function sigma factor, regulates the biosynthesis of pyoverdine, a siderophore enriched in cluster II (Fig. 3*A* and Dataset S4). *pvdS* is negatively regulated by Fur and is derepressed under iron-deficient conditions (39). The Fur or PvdS motif was enriched in the promoter region of the genes suppressed by both plant immunity and iron (Fig. 4*A*; the cluster of genes marked with red in the dendrogram), including the *pvdS* gene itself (Fur: 17.4-fold over-enriched, $P = 6.22e^{-9}$; PvdS: 15.2-fold over-enriched; $P = 1.85e^{-9}$; hypergeometric test) (Fig. 4*A*). RT-qPCR analysis confirmed our RNA-seq data that *pvdS* expression was suppressed by AvrRpt2-triggered ETI (Fig. 4*B*). These results pinpointed the Fur–PvdS pathway as a potential target of plant immunity for impeding bacterial growth. Moreover, three of five bacterial sigma factors directly regulated by Fur (41) were strongly induced *in planta* and were suppressed by both flg22-PTI and AvrRpt2-ETI (Fig. S6), suggesting that plant immunity might broadly target iron-related sigma factors to manipulate bacterial iron metabolism.

***pvdS* Has a Causal Impact on Bacterial Growth *in Planta*.** We found suppression of the PvdS pathway by both PTI and ETI striking (Figs. 2*C* and 3 *A* and *C*). To examine whether the manipulation of the PvdS regulatory pathway has causal effects on bacterial growth *in planta*, we generated a *Pto* AvrRpt2 strain that constitutively expresses *pvdS* (AvrRpt2 *pvdS*-ox) to counteract the suppression of *pvdS* expression by ETI (Fig. 4*B*). AvrRpt2 *pvdS*-ox grew 12-fold more than *Pto* AvrRpt2 (AvrRpt2 EV) in Col-0 plants, whereas these two strains grew at a similar level in *rps2 rpm1*-mutant plants, which do not trigger ETI (Fig. 4*C* and Fig. S7). Thus, high *pvdS* expression confers *Pto* tolerance against AvrRpt2-triggered ETI.

Regulation of *pvdS* in Plants Is Independent of Iron Concentration. Since *pvdS* suppression occurs under iron-rich conditions in vitro, we tested the possibility that ETI suppressed *pvdS* expression by increasing apoplastic iron. By coinoculating bacteria with Fe-citrate, we showed that iron did not influence *pvdS* expression even at a concentration detrimental for bacterial growth in plants (Fig. 5 *A* and *B*). Furthermore, iron content in apoplastic and intracellular fluid did not change upon flg22 treatment or ETI triggered by bacterial infection (Fig. 5 *C* and *D*). Collectively, these data suggest that altered iron availability is unlikely to be the cause of changes in *pvdS* expression resulting from plant immunity and that plant immunity influences *pvdS* expression by means other than directly regulating iron concentrations.

Discussion

Studies of plant disease resistance in the past few decades have revealed two major forms of plant innate immunity, PTI and

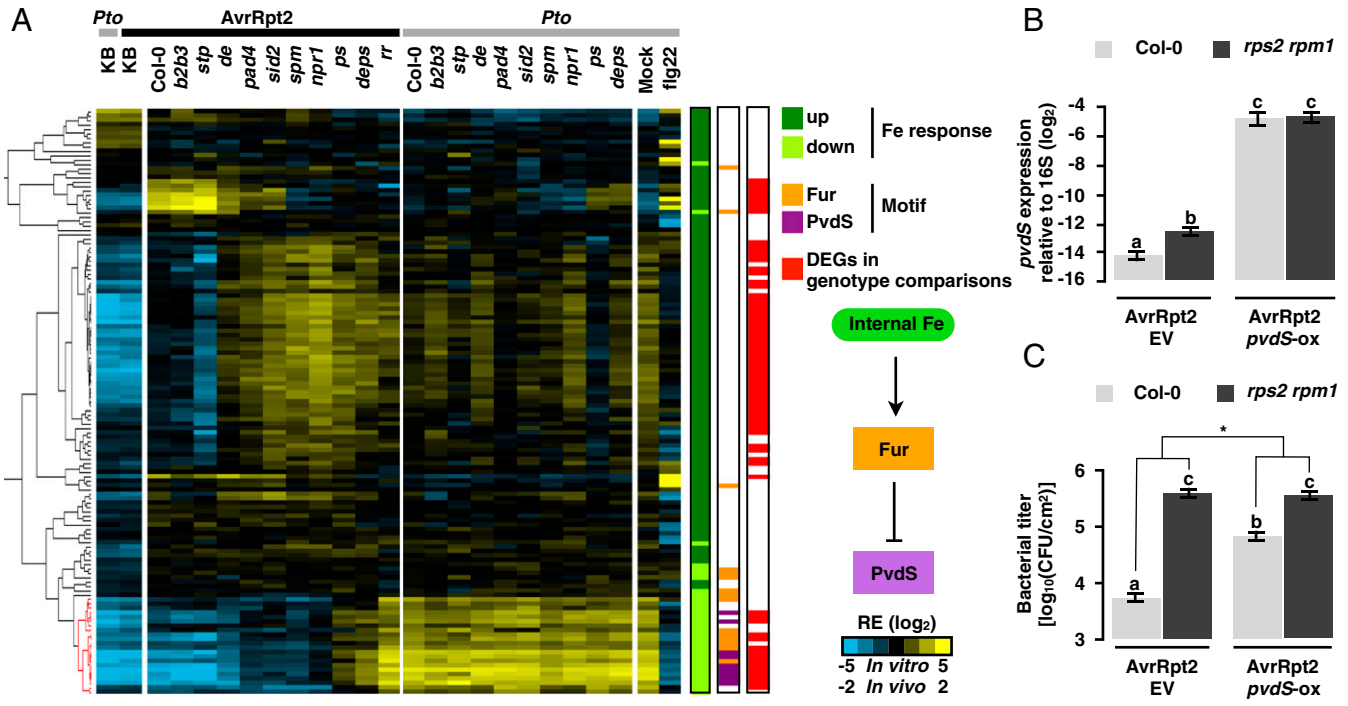

Fig. 4. Iron-related genes of *Pto* are targeted by plant immunity. (*A*) Hierarchical clustering of the relative expression (RE) of *Pto* genes previously reported as iron responsive (39). Iron-inducible and iron-repressive genes are represented by dark and light green marks, respectively ($P < 0.05$). The red marks represent *Pto* AvrRpt2 genes differentially expressed in at least one of the pairwise comparisons between Col-0 plants and the defense-mutant plants. Binding motifs of Fur and PvdS are represented by orange and purple marks, respectively. *Pto* and *Pto* AvrRpt2 are represented by gray and black marks, respectively. (*B*) RT-qPCR analysis of *pvdS* expression of *Pto* AvrRpt2 carrying an empty vector (EV) or *Pto* AvrRpt2 *pvdS*-ox ($OD_{600} = 0.5$) normalized to 16S in Col-0 or *rps2 rpm1* plants at 6 hpi. (*C*) Growth of *Pto* AvrRpt2 EV or *Pto* AvrRpt2 *pvdS*-ox ($OD_{600} = 0.001$) in Col-0 or *rps2 rpm1* plants at 48 hpi. In *B* and *C*, the mean ± SEM was calculated by using a mixed linear model (*B*: $n = 4$ biological replicates from four independent experiments, *C*: $n = 72$ and 48 biological replicates from six and four independent experiments for Col-0 and *rps2 rpm1*, respectively). Different letters indicate statistically significant differences (adjusted $P < 0.01$; Benjamini–Hochberg method). The asterisk indicates a statistically significant difference in the host genotype effect in the bacterial strains ($P = 6.61E\text{-}08$; two-tailed Student's *t* test).

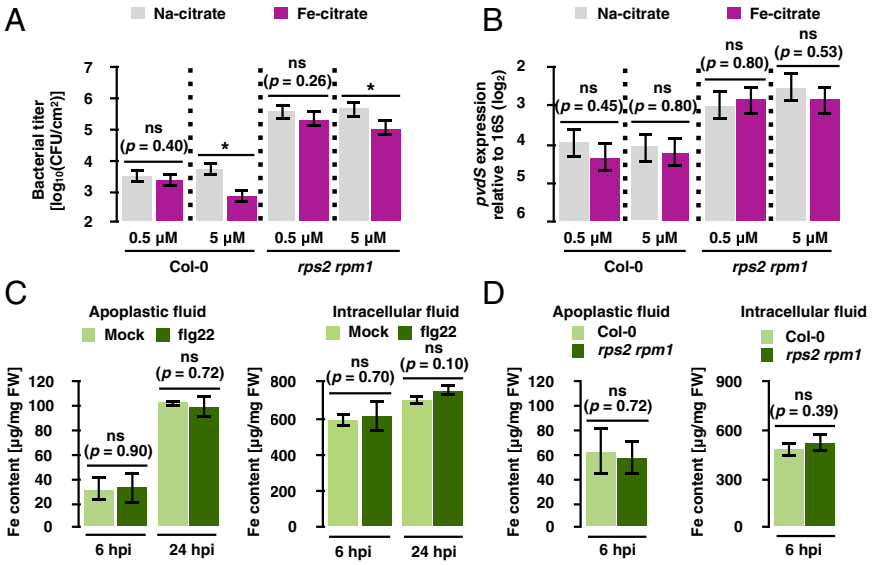

Fig. 5. Iron content in the apoplast does not explain *pvdS* expression and *Pto* growth. (*A*) Growth assay of *Pto* AvrRpt2 in Col-0 and *rps2 rpm1* plants at 48 hpi. The bacterial suspension (OD_{600} = 0.001) was coinfiltrated with Na-citrate or Fe-citrate. (*B*) RT-qPCR analysis of *pvdS* expression in *Pto* AvrRpt2 in Col-0 and *rps2 rpm1* plants at 6 hpi. Bacterial suspension (OD_{600} = 0.5) was coinfiltrated with Na-citrate or Fe-citrate. Error bars in *A* and *B* represent means and SEs calculated from independent experiments using a mixed linear model (*A*: $n = 3$, *B*: $n = 6$). Asterisks indicate statistically significant differences (adjusted *P* value < 0.01). ns, not significant (adjusted *P* values are shown). (*C*) Iron content in apoplastic and intracellular fluids extracted from Col-0 plants sprayed with 1 μM flg22 or water (Mock) at the indicated time points. (*D*) Iron content in apoplastic and intracellular fluids extracted from Col-0 or *rps2 rpm1* plants infiltrated with *Pto* AvrRpt2 (OD_{600} = 0.5). Error bars in *C* and *D* represent means and SEs calculated from three independent experiments. ns, not significant (*P* values are shown; two-tailed Student's *t* test).

ETI. PTI and ETI are highly effective in restricting pathogen growth. However, how PTI and ETI halt pathogen growth remains an outstanding question that has been difficult to elucidate. In this study, using *in planta* bacterial RNA-seq analysis, we were able to link the activation of various immune-signaling pathways to specific changes in global bacterial gene expression, thereby defining the immune-responsive sector of the *Pto* transcriptome (Figs. 2 and 3). We found that the expression pattern of the immune-responsive sector genes at an early time point of infection is tightly linked to bacterial growth at a later time point (Fig. 3*B*). Importantly, among the immune-responsive sector genes is *pvdS* (Fig. 4), a transcriptional regulator previously known for its role in regulating iron responses (34). We found that overexpression of *pvdS* partially counters AvrRpt2-triggered ETI (Fig. 4*C*), exemplifying a causal role of the immune-responsive sector genes in mediating bacterial growth inhibition during plant immunity.

The T3SS and T3Es have long been known as essential virulence factors of bacterial pathogens (4). Suppression of T3E translocation and T3SS expression by PTI has been proposed to be an attractive mechanism of attenuating pathogen virulence capacity during plant immunity (16). Remarkably, however, our *in planta* transcriptome analysis revealed that PTI has a much broader impact on bacterial metabolism beyond the T3SS, including fundamental processes of life, such as protein translation (Fig. 2*C*), suggesting that bacterial growth inhibition during PTI may be caused by the alteration of multiple bacterial processes other than or in addition to T3SS suppression. Because our bacterial transcriptome profiling was conducted at an early time point before bacterial population densities diverged in different samples (Fig. S4), these broad effects are not a consequence of differential bacterial population densities per se. Furthermore, although ETI also can effectively halt bacterial growth, our data suggested that ETI has a narrower impact on the bacterial transcriptome. Most notably, ETI did not markedly affect the expression of T3SS genes (Figs. 2*C* and 3*A*; see *Pto* vs. *Pto* AvrRpt2 in Col-0 plants or Col-0 vs. *rps2 rpm1* plants in *Pto* AvrRpt2) (20). This is consistent with the notion that PTI, but not ETI, invariably blocks T3Es translocation into host plant cells (16, 20). It should be pointed out that, due to the cost of profiling a large number of tissue samples, we had to restrict sampling to a single time point in this study. Therefore, our study cannot exclude the possibility that the different effects observed between PTI and ETI could be partially due to different kinetics of immune activation during PTI and ETI. Transcriptome analyses at multiple time points would be an important future direction to understand the dynamic transcriptome responses of bacteria in plants.

Plant defense hormone pathways (e.g., the SA, JA, and ET pathways) are known to contribute redundantly to plant transcriptional reprogramming and bacterial growth suppression (29, 42). Our RNA-seq data showed that these hormone pathways also redundantly affect the *Pto* bacterial transcriptome (Fig. 3*A*). How different hormone pathways converge on a similar impact on bacterial gene expression remains to be investigated. One possibility is that different hormone pathways lead to the same immune output/signal that ultimately affects the bacterial transcriptome. Another possibility is that different immune pathways have distinct immune outputs/signals, but they ultimately affect the bacterial transcriptome in a similar fashion. The identity of such immune outputs/signals (i.e., changes in apoplastic environments) remains obscure and is a subject for future experimentation.

Our bacterial transcriptome data provided some clues for the changes in apoplastic environments during immune activation. We found that both PTI and ETI commonly suppress the expression of bacterial iron-associated genes, and this was associated with bacterial growth inhibition (Fig. 2*C*). This finding enabled us to uncover that the bacterial sigma factor gene *pvdS* plays a causal role in mediating part of bacterial growth inhibition during AvrRpt2-triggered ETI (Fig. 4*C*). PvdS is a widely conserved global iron-response regulator in plant/animal pathogenic and commensal bacteria (43), implying that the suppression of bacterial iron-acquisition pathways may be a general

strategy for plant immunity to control bacterial growth *in planta*. Besides the interesting ability of *pvdS* overexpression to partially counter AvrRpt2-triggered ETI, future research should examine whether PvdS and related sigma factors are also required for basic *Pto* virulence in plants. *Pto* has four other sigma factor genes that are responsive to iron starvation (41), at least two of which, PSPTO_1203 and PSPTO_1209, were suppressed by plant immunity (Fig. S6). Understanding the roles of these sigma factors in basic bacterial virulence is an important future direction.

Iron is a two-faced element for bacterial growth: It is essential for biological processes, but in excess iron is toxic (44). It is well studied that animal hosts regulate iron availability in both directions, iron sequestration and intoxication, to inhibit pathogen growth (45). It is also known that some bacterial pathogens have evolved mechanisms to avoid host-mediated iron regulation (45). Thus, regulation of iron homeostasis seems to be under selective pressure during coevolution between hosts and bacteria. However, this study could not establish whether and how plant immunity modulates *Pto* iron homeostasis during infection. Because PvdS-target genes may function in cellular processes beyond iron homeostasis (43), it is possible that bacterial processes regulated by PvdS other than iron homeostasis may also be critical for *in planta Pto* growth. A previous study suggested that the iron concentration of *A. thaliana* apoplast was not a limiting factor for bacterial growth (46). It was also shown that a PvdS-regulated siderophore, pyoverdine, and other high-affinity iron-scavenging systems are dispensable for *Pto* pathogenesis (47). Taking these findings together with our observation that iron coinfiltration did not promote *Pto* growth in plants (Fig. 5*A*), we infer that iron limitation in the apoplast unlikely explains poor *Pto* growth under ETI. On the other hand, PTI and ETI clearly suppressed *Pto* genes that are known to be suppressed by iron supplementation in vitro (Fig. 4*A*), suggesting that plant immunity causes an iron-rich–like response in bacteria. However, our data suggested that PTI and ETI do not change the iron content in the plant apoplast (Fig. 5), indicating that plant immunity likely influences bacterial iron-responsive genes independently of iron content. In this regard, it is tempting to speculate that plants may secrete an iron-mimicking compound that misregulates the Fur–PvdS regulon to trick bacteria into an iron-starved state without drastically changing the apoplastic iron content, which otherwise might cause collateral damage in plant growth and reproduction. Future research is needed to test the hypothesis that production of iron-mimicking compounds to perturb bacterial iron response might be an antibacterial strategy in plant immunity.

Beyond uncovering an enigmatic transcriptome response of *Pto* to plant immunity, our *in planta* bacterial RNA-seq pipeline opens an exciting possibility to study the *in planta* transcriptomes of a variety of bacterial species and bacterial communities naturally associated with plants. Healthy plants are colonized by multitudes of microorganisms, and plant immunity has been shown to be important for modulating commensal or beneficial relationships with microbial colonizers (48). How plant immunity shapes the transcriptomic and metabolic dynamics of diverse plant-associated bacterial species to maintain microbiome homeostasis remains an outstanding question. Combined with other methodologies, the *in planta* bacterial transcriptome approach reported here has potential to provide untapped opportunities to holistically understand the interactions between host immunity and microbiota.

Materials and Methods

Plant Materials and Growth Conditions. The *A. thaliana* accession Col-0 was the background of all *A. thaliana* mutants used in this study. The *A. thaliana* mutants *rpm1-3 rps2-101C* (49), *cyp79b2 cyp79b3* (37), *npr1-1* (50), and *stp1 stp13* (51) and combinatorial mutants (29) of the *A. thaliana* mutants *dde2-2* (52), *ein2-1* (53), *pad4-1* (54), and *sid2-2* (55) were described previously. The double mutant *sid2-2 pmr4-1* was generated by standard genetic crosses (56). Plants were grown in a chamber at 22 °C with a 10-h light period and 60% relative humidity for 24 d and then in another chamber at 22 °C with a 12-h light period and 60% relative humidity. For all experiments, 31- to 33-d-old plants were used.

Bacterial Strains. *Pto* DC3000 carrying empty vector (pLAFR), *avrRpt2* (pLAFR) (57), and *avrRps4* (pVSP61) (58) and effector-deficient mutant *Pto* D36E (28) were described previously.

Accession Numbers. The accession numbers for the genes discussed in this article are as follows: *AtACTIN2* (At2g18780), *AtPR1* (AT2G14610), *AtDDE2* (AT5G42650), *AtEIN2* (AT5G03280), *AtPAD4* (AT3G52430), *AtSID2* (AT1G74710), *AtNPR1* (AT1G64280), *AtPMR4* (AT4G03550), *AtSTP1* (AT1G11260), *AtSTP13* (AT5G26340), *AtCYP79B2* (AT4G39950), *AtCYP79B3* (AT2G22330), *AtRPS2* (AT3G03600), *AtRPM1* (AT3G07040), *pvdS* (PSPTO_2133), *hrpL* (PSPTO_1404), *avrPto* (PSPTO_4001), *cmaA* (PSPTO_4709), *gapA* (PSPTO_1287), *katB* (PSPTO_3582), *katG* (PSPTO_4530), *gyrA* (PSPTO_1745). *A. thaliana* and *Pto* accession numbers were based on The Arabidopsis Information Resource and The Pseudomonas Genome Database, respectively.

In Vitro Bacterial Cultures for RNA-Seq. Bacteria were grown in either King's B medium (1% proteose peptone, 1.5% glycerol, 8.6 mM K_2HPO_4, 5 mM $MgSO_4$, pH 6.9) or type III-inducible medium (31) [50 mM KH_2PO_4, 7.6 mM $(NH_4)_2SO_4$, 1.7 mM NaCl, 1.7 mM $MgCl_26H_2O$, 10 mM fructose, pH 5.7] to OD_{600} = 0.65 (exponential phase) at 28 °C. Upon harvesting bacterial cells, 0.1 volumes of 5% phenol and 95% ethanol were added to the culture, which was then resuspended and centrifuged, followed by total RNA extraction for RNA-seq of the bacterial pellet.

Elicitor Pretreatment. One day before bacterial infection, leaves were sprayed with H_2O (mock treatment), 1 μM flg22 (EZBiolab), 100 μg/mL chitosan (Sigma), or 50 μM SA (Duchefa Biochemie).

Bacterial Infection and Sampling. *Pto* stains were cultured in King's B medium at 28 °C. Bacteria were harvested by centrifugation and resuspended in sterile water to an OD_{600} of 0.5 (~2.5×10^8 cfu/mL). In total, 80–100 *A. thaliana* leaves (four leaves per plant) were syringe-inoculated with bacterial suspensions using a needleless syringe. The infected leaves were harvested at 6 hpi, immediately frozen in liquid nitrogen, and stored at −80 °C.

Establishment of a Bacterial Isolation Buffer. The bacterial isolation buffer needs to be able to fix bacterial metabolism, protect bacterial RNA from degradation, and separate bacterial cells from plant cells. We first tested a commonly used solution containing 9.5% ethanol and 0.5% phenol. This could protect bacterial RNA when bacteria were incubated alone but not when mixed with crushed plant leaves (Fig. S1*C*). Adding the reducing agent Tris(2-carboxyethyl)phosphine (TCEP; Sigma) to a final concentration of 25 mM protected bacterial RNA in the mixed condition in a pH-dependent manner: Buffers with lower pH protected bacterial RNA better (Fig. S1*C*). We determined pH 4.5 as an optimal condition, where both RNA protection and bacterial enrichment could be sufficiently accomplished. Incubating bacterial cells in this buffer did not affect bacterial transcriptome patterns, suggesting that this buffer fixed bacterial metabolism (Fig. S1*D*).

Bacterial Isolation. Frozen infected leaves (80–100 leaves) were crushed with 8–10 metal beads (4 mm) by manually shaking the tube. To isolate bacterial cells, 30 mL of fresh bacterial isolation buffer was added to the crushed leaves and mixed thoroughly by vigorous manual shaking and vortexing. All subsequent processes were done on ice or in a cold room (4 °C). The sample was incubated for 20 h with mild shaking. After 20 h of incubation, the sample was passed through a 6-μm filter to remove large plant debris. The flowthrough was centrifuged at 3,200 × *g* for 20 min to pellet plant and bacterial cells. The supernatant was carefully removed, and the pellet was resuspended in 900 μL of a buffer containing 9.5% EtOH and 0.5% phenol. The suspension was centrifuged at 2,300 × *g* for 20 min to obtain a two-layered pellet (a white layer on the top and a green layer on the bottom). The top layer of the pellet (bacterial cells) was resuspended by pipetting while keeping the bottom layer (plant cells) intact. Then, the liquid phase, in which the top layer was suspended, was transferred to a new tube. Bacterial cells were collected by centrifuging at 10,000 × *g* for 2 min and were resuspended in 1 mL of TriFast (Peqlab).

RNA Extraction. The TriFast solution was mixed with 200 μL of chloroform, and the aqueous phase was isolated by centrifugation (typically 400 μL). The aqueous phase was mixed with 200 μL (half volume) of ethanol and then

applied to the column of RNAqueous kit (Ambion). RNA was eluted in 30 μL of RNase-free water following the manufacturer's protocol and treated with 2 U of TURBO DNase (Ambion) for 30 min at 37 °C. Then, plant rRNA was removed using the Ribo-Zero plant kit (Epicentre) following the manufacturer's protocol. Input RNA amount ranged from 2.5–5 μg depending on the yield of RNA after DNase treatment. Plant rRNA-depleted RNA was purified and concentrated with the RNeasy MinElute kit (Qiagen).

cDNA Library Generation and RNA-Seq. cDNA libraries were generated with the Ovation Complete Prokaryotic RNA-seq kit 1-8 (NuGEN), following the manufacturer's protocol with some modifications. Ten nanograms of plant rRNA-depleted RNA was used as input. DNA fragmentation was conducted with a Covaris S-Series instrument. cDNA libraries were subjected to RNA-seq at the Max Planck Genome Centre Cologne using an Illumina HiSeq 3000 system with 150-bp strand-specific single-end read, resulting in ∼10 million reads per sample. The Illumina CASAVA pipeline (version 1.8.2) was used for base calling, and cutadapt (59) was used for discarding reads containing the Illumina adaptor sequences. The resulting reads were mapped onto the *Pto* DC3000 genome/coding sequence (CDS) (*Pseudomonas* Genome Database) and the *A. thaliana* genome (TAIR10) using Bowtie2 (60) and TopHat2 (61), respectively. Mapped reads were counted with the Python package HTSeq. (62). The RNA-seq data used in this study are deposited in the National Center for Biotechnology Information Gene Expression Omnibus database (accession no. GSE103442).

Differential Gene-Expression Analysis. The statistical analysis of the RNA-seq data was performed in the R environment. Genes with zero counts in at least one of the samples were excluded. The count data of the remaining genes were normalized and log-transformed by the function calcNormFactors [trimmed mean of M-values (TMM) normalization] in the package edgeR (63) and the function voomWithQualityWeights in the package limma (64), respectively. Density plot analysis, carried out with the function plotDensities in the package limma, showed that TMM normalization successfully normalized the read-count distribution of each sample (Fig. S2*C*). To each gene, a linear model was fit by using the function lmFit in the limma package with the following terms: Sgtr = GTgt + Rr + ϵgtr, where S is the $\log_2$ count per million, GT is the host genotype:*Pto* strain interaction and the random factors, R is the biological replicate, and ϵ is the residual. The eBayes function in the limma package was used for variance shrinkage in the calculation of the *P* values, which was then used to calculate the false discovery rate (FDR; the Storey's *q*-values) using the qvalue function in the qvalue package (65). All normalized mean expression values ($\log_2$ counts per million) of bacterial genes are shown in Dataset S6. To extract genes with significant expression changes, the cutoff of *q*-value <0.01 and $|\log_2$ fold change$| > 2$ was applied. The prcomp function was used for principal component analysis. The multidimensional scaling (MDS) plot was created with the plotMDS function in the package edgeR. Hierarchical clustering was done using the dist and hclust functions in the R environment or using Cluster3.0 software (66). Heatmaps were created with the heatmap3 function in the R environment or using TreeView (67). For the distance heat map, the distances were calculated using the dist function in R environment after estimating a mean-dispersion relationship of the data using the estimateDispersions function with method = 'blind' and transforming the variance with the varianceStabilizingTransformation function in the DESeq2 package (68). Enriched GO terms were identified using the BiNGO plugin for Cytoscape (69).

Quality Assessment of RNA-Seq Data. There was certain variation in the bacterial enrichment rate among samples, and some sequence reads were mapped to neither the *Pto* nor the *A. thaliana* genome due to low quality or contaminations ("Else" in Fig. 1*C*). However, hierarchical clustering of RNA-seq data showed that the bacterial enrichment rate and the sequence depth did not explain the transcriptome pattern (Fig. S2*A*), suggesting that there are no systematic biases caused by our enrichment method.

***In Planta* Bacterial Transcriptome Method Based on Customized Probes.** *Pto* DC3000 was grown in King's B medium at 30 °C. Plants were grown in a chamber with a 12-h light period, 23 °C temperature during the day and 21 °C at night.

Two leaves from 3- to 4.5-wk-old *A. thaliana* plants were infiltrated with either 0.005% DMSO (mock treatment) or 500 nM flg22 using a needleless syringe. Plants were inoculated with a bacterial suspension at an OD_{600} of 0.75 (∼10^9 cfu/mL) of *Pto* DC3000 at 20 h post infiltration. Seven hours after *Pto* DC3000 inoculation, leaves were collected for RNA extraction.

RNA was extracted using the TRIzol reagent (Thermo Fisher Scientific) and the Direct-zol RNA Miniprep kit (Zymo Research). Purified RNA was treated with 10 U of RNase-free DNase I (Roche Applied Science), after which RNA was purified a second time with the Direct-zol RNA Miniprep kit. Nonorganellar 18S and 28S rRNAs, and poly(A) mRNAs were depleted using the MICROBEnrich kit (Thermo Fisher Scientific). RNA quality was evaluated using the Agilent 2100 BioAnalyzer, and RNA concentration was determined using the Qubit RNA HS assay kit (Thermo Fisher Scientific).

RNA-seq libraries were prepared using the Ovation *Arabidopsis* RNA-seq system 1-16 (NuGEN) with two modifications to the manufacturer's protocol. First-strand cDNA synthesis used only the first-strand primer random mix (the oligo dT primer mix was omitted), while on strand selection II, custom insert-dependent adapter cleavage probes (InDA-C; currently referred to as "AnyDeplete") with specificity to highly abundant *A. thaliana* chloroplast and nuclear transcripts (361 probes) and *Pto* DC3000 rRNAs (65 probes; 1 μL of each 2-μM probe mixture was used; Dataset S7) were added to the mixture of *A. thaliana* cytoplasmic, chloroplast, and mitochondrial rRNA custom probes that are included with the kit.

Libraries were pooled and sequenced in the Illumina HiSeq. 2500 system using HiSeq SBS reagents (version 4) to obtain 50-bp single reads. Base calling was done by the Illumina Real Time Analysis software (RTA version 1.18.64).

Primer Information. The list of primers used in this study is provided in Dataset S8.

RT-qPCR Analysis. RT-qPCR was performed using the SuperScript One-Step RT-PCR system kit (Invitrogen). As inputs, 3 ng and 300 ng of DNase-treated RNA extracted from infected leaves were used for analyzing plant and bacterial genes, respectively.

Generation of *pvdS*-Overexpressing *Pto*. The *pvdS* CDS was amplified from *Pto* genomic DNA by PCR with the primers pvdS_F and pvdS_R. The amplified fragment was linked with the DNA amplified from pLMB426 plasmid (70) with the primers pLMB426_F and pLMB426_R under the Ptac promoter, using an in-fusion cloning kit (Clontech) to make the circular plasmid. The DNA amplified from pLMB426 plasmid with the primers pLMB426_F2 and pLMB426_R2 was digested with XhoI and ligated to generate the empty vector. The resulted plasmid was transformed into *Pto* AvrRpt2 by a triparental mating using the helper strain carrying pRK600 and was selected with 40 μg/mL rifampicin, 10 μg/mL tetracycline, and 50 μg/mL gentamycin.

Bacterial Growth Assay. Bacterial growth assays were performed as described previously (29). Bacteria-infected plants were kept in a chamber at 22 °C with a 12-h light period and 60% relative humidity. For the Fe coinfiltration study, Na-citrate or Fe-citrate (Sigma) was dissolved in a bacterial suspension at the desired concentration before syringe infiltration.

Extraction of Apoplastic and Intracellular Fluids and Iron Measurement. Extraction of apoplastic and intracellular fluid was performed following a previous publication with slight modifications (71). Leaves from 4-wk-old plants were washed and vacuum infiltrated with cold water twice for 2 min. Apoplastic fluids were collected by centrifugation at 3,000 × *g* for 5 min in 50-mL tubes. The leaves were then frozen at −80 °C overnight and thawed at room temperature for 20 min. Intracellular fluids were collected from the frozen leaves by centrifugation at 12,000 × *g* for 10 min. For iron measurement, HNO_3 and H_2O_2 were added to the apoplastic and intracellular fluids for final concentrations of 1% (vol/vol), followed by heating at 95 °C for 10 min. The precipitate was removed by centrifugation at 12,000 × *g* for 5 min. The remaining solutions were filtered through 5-μm filters (Millex-SV syringe filter unit; Millipore), followed by measurement with an inductively coupled plasma mass spectrometer (ICP-MS). The concentration of the different elements was determined using an Agilent 7700 ICP-MS (Agilent Technologies), strictly following the manufacturer's instructions.

ACKNOWLEDGMENTS. We thank Dr. Barbara Kracher for bioinformatics support, Dr. Phillip Poole for providing pLMB426 plasmid, Dr. Alan Collmer for providing the *Pto* DC3000 D36E strain, Sajjad Khani for initiating a preliminary protocol of *in planta* bacterial RNA-seq with bacterial isolation, John Paul Jerome for initiating a preliminary protocol of *in planta* bacterial RNA-seq without bacterial isolation, Dr. Bruno Huettel and the Max Planck Genome Centre Cologne for technical help in next-generation sequencing, the University of Cologne Biocenter MS Platform for ICP-MS analysis, and Dr. Paul Schulze-Lefert for critical reading of the manuscript. This work was supported by the Max Planck Society and Deutsche Forschungsgemeinschaft Grant SFB670 (to K.T.), Gordon and Betty Moore Foundation Grant GBMF 3037 and NIH Grant GM109928 (to S.Y.H.), a predoctoral fellowship from the Nakajima Foundation (to T.N.), and a postdoctoral fellowship from the Alexander von Humboldt Foundation (to Y.W.).

1. Jones JDG, Dangl JL (2006) The plant immune system. *Nature* 444:323–329.
2. Couto D, Zipfel C (2016) Regulation of pattern recognition receptor signalling in plants. *Nat Rev Immunol* 16:537–552.
3. Tang D, Wang G, Zhou JM (2017) Receptor kinases in plant-pathogen interactions: More than pattern recognition. *Plant Cell* 29:618–637.
4. Büttner D, He S-Y (2009) Type III protein secretion in plant pathogenic bacteria. *Plant Physiol* 150:1656–1664.
5. Cui H, Tsuda K, Parker JE (2015) Effector-triggered immunity: From pathogen perception to robust defense. *Annu Rev Plant Biol* 66:487–511.
6. Tsuda K, Katagiri F (2010) Comparing signaling mechanisms engaged in pattern-triggered and effector-triggered immunity. *Curr Opin Plant Biol* 13:459–465.
7. Fones H, Preston GM (2013) The impact of transition metals on bacterial plant disease. *FEMS Microbiol Rev* 37:495–519.
8. Aslam SN, et al. (2008) Bacterial polysaccharides suppress induced innate immunity by calcium chelation. *Curr Biol* 18:1078–1083.
9. Quiñones B, Dulla G, Lindow SE (2005) Quorum sensing regulates exopolysaccharide production, motility, and virulence in Pseudomonas syringae. *Mol Plant Microbe Interact* 18:682–693.
10. Vargas P, et al. (2013) Plant flavonoids target Pseudomonas syringae pv. tomato DC3000 flagella and type III secretion system. *Environ Microbiol Rep* 5:841–850.
11. Glickmann E, et al. (1998) Auxin production is a common feature of most pathovars of Pseudomonas syringae. *Mol Plant Microbe Interact* 11:156–162.
12. Mittal S, Davis KR (1995) Role of the phytotoxin coronatine in the infection of Arabidopsis thaliana by Pseudomonas syringae pv. tomato. *Mol Plant Microbe Interact* 8: 165–171.
13. Toruño TY, Stergiopoulos I, Coaker G (2016) Plant-pathogen effectors: Cellular probes interfering with plant defenses in spatial and temporal manners. *Annu Rev Phytopathol* 54:419–441.
14. Chen L-Q, et al. (2010) Sugar transporters for intercellular exchange and nutrition of pathogens. *Nature* 468:527–532.
15. Xin X-F, et al. (2016) Bacteria establish an aqueous living space in plants crucial for virulence. *Nature* 539:524–529.
16. Crabill E, Joe A, Block A, van Rooyen JM, Alfano JR (2010) Plant immunity directly or indirectly restricts the injection of type III effectors by the Pseudomonas syringae type III secretion system. *Plant Physiol* 154:233–244.
17. Anderson JC, et al. (2014) Decreased abundance of type III secretion system-inducing signals in Arabidopsis mkp1 enhances resistance against Pseudomonas syringae. *Proc Natl Acad Sci USA* 111:6846–6851.
18. Yamada K, Saijo Y, Nakagami H, Takano Y (2016) Regulation of sugar transporter activity for antibacterial defense in Arabidopsis. *Science* 354:1427–1430.
19. Tsuda K, Sato M, Glazebrook J, Cohen JD, Katagiri F (2008) Interplay between MAMP-triggered and SA-mediated defense responses. *Plant J* 53:763–775.
20. Nomura K, et al. (2011) Effector-triggered immunity blocks pathogen degradation of an immunity-associated vesicle traffic regulator in Arabidopsis. *Proc Natl Acad Sci USA* 108:10774–10779.
21. Yu X, et al. (2013) Transcriptional responses of Pseudomonas syringae to growth in epiphytic versus apoplastic leaf sites. *Proc Natl Acad Sci USA* 110:E425–E434.
22. Yu X, et al. (2014) Transcriptional analysis of the global regulatory networks active in Pseudomonas syringae during leaf colonization. *MBio* 5:e01683-14.
23. Chapelle E, et al. (2015) A straightforward and reliable method for bacterial in planta transcriptomics: Application to the Dickeya dadantii/Arabidopsis thaliana pathosystem. *Plant J* 82:352–362.
24. Chatnaparat T, Prathuangwong S, Lindow SE (2016) Global pattern of gene expression of Xanthomonas axonopodis pv. glycines within soybean leaves. *Mol Plant Microbe Interact* 29:508–522.
25. Mindrinos M, Katagiri F, Yu GL, Ausubel FM (1994) The A. thaliana disease resistance gene RPS2 encodes a protein containing a nucleotide-binding site and leucine-rich repeats. *Cell* 78:1089–1099.
26. Bent AF, et al. (1994) RPS2 of Arabidopsis thaliana: A leucine-rich repeat class of plant disease resistance genes. *Science* 265:1856–1860.
27. Gassmann W, Hinsch ME, Staskawicz BJ (1999) The Arabidopsis RPS4 bacterial-resistance gene is a member of the TIR-NBS-LRR family of disease-resistance genes. *Plant J* 20:265–277.
28. Wei H-L, et al. (2015) Pseudomonas syringae pv. tomato DC3000 type III secretion effector polymutants reveal an interplay between HopAD1 and AvrPtoB. *Cell Host Microbe* 17:752–762.
29. Tsuda K, Sato M, Stoddard T, Glazebrook J, Katagiri F (2009) Network properties of robust immunity in plants. *PLoS Genet* 5:e1000772.
30. Papenfort K, Bassler BL (2016) Quorum sensing signal-response systems in Gram-negative bacteria. *Nat Rev Microbiol* 14:576–588.
31. Huynh TV, Dahlbeck D, Staskawicz BJ (1989) Bacterial blight of soybean: Regulation of a pathogen gene determining host cultivar specificity. *Science* 245:1374–1377.
32. Tang X, Xiao Y, Zhou J-M (2006) Regulation of the type III secretion system in phytopathogenic bacteria. *Mol Plant Microbe Interact* 19:1159–1166.
33. Hauck P, Thilmony R, He SY (2003) A Pseudomonas syringae type III effector suppresses cell wall-based extracellular defense in susceptible Arabidopsis plants. *Proc Natl Acad Sci USA* 100:8577–8582.
34. Brooks DM, et al. (2004) Identification and characterization of a well-defined series of coronatine biosynthetic mutants of Pseudomonas syringae pv. tomato DC3000. *Mol Plant Microbe Interact* 17:162–174.
35. Zipfel C, et al. (2004) Bacterial disease resistance in Arabidopsis through flagellin perception. *Nature* 428:764–767.
36. Mikkelsen MD, Hansen CH, Wittstock U, Halkier BA (2000) Cytochrome P450 CYP79B2 from Arabidopsis catalyzes the conversion of tryptophan to indole-3-acetaldoxime, a precursor of indole glucosinolates and indole-3-acetic acid. *J Biol Chem* 275:33712–33717.
37. Zhao Y, et al. (2002) Trp-dependent auxin biosynthesis in Arabidopsis: Involvement of cytochrome P450s CYP79B2 and CYP79B3. *Genes Dev* 16:3100–3112.
38. Rajniak J, Barco B, Clay NK, Sattely ES (2015) A new cyanogenic metabolite in Arabidopsis required for inducible pathogen defence. *Nature* 525:376–379.
39. Bronstein PA, et al. (2008) Global transcriptional responses of Pseudomonas syringae DC3000 to changes in iron bioavailability in vitro. *BMC Microbiol* 8:209.
40. Llamas MA, Imperi F, Visca P, Lamont IL (2014) Cell-surface signaling in Pseudomonas: Stress responses, iron transport, and pathogenicity. *FEMS Microbiol Rev* 38:569–597.
41. Markel E, et al. (2013) Regulons of three Pseudomonas syringae pv. tomato DC3000 iron starvation sigma factors. *Appl Environ Microbiol* 79:725–727.
42. Hillmer RA, et al. (2017) The highly buffered Arabidopsis immune signaling network conceals the functions of its components. *PLoS Genet* 13:e1006639.
43. Swingle B, et al. (2008) Characterization of the PvdS-regulated promoter motif in Pseudomonas syringae pv. tomato DC3000 reveals regulon members and insights regarding PvdS function in other pseudomonads. *Mol Microbiol* 68:871–889.
44. Verbon EH, et al. (2017) Iron and immunity. *Annu Rev Phytopathol* 55:355–375.
45. Chandrangsu P, Rensing C, Helmann JD (2017) Metal homeostasis and resistance in bacteria. *Nat Rev Microbiol* 15:338–350.
46. O'Leary BM, et al. (2016) Early changes in apoplast composition associated with defence and disease in interactions between Phaseolus vulgaris and the halo blight pathogen Pseudomonas syringae Pv. phaseolicola. *Plant Cell Environ* 39:2172–2184.
47. Jones AM, Wildermuth MC (2011) The phytopathogen Pseudomonas syringae pv. tomato DC3000 has three high-affinity iron-scavenging systems functional under iron limitation conditions but dispensable for pathogenesis. *J Bacteriol* 193:2767–2775.
48. Hacquard S, Spaepen S, Garrido-Oter R, Schulze-Lefert P (2017) Interplay between innate immunity and the plant microbiota. *Annu Rev Phytopathol* 55:565–589.
49. Mackey D, Belkhadir Y, Alonso JM, Ecker JR, Dangl JL (2003) Arabidopsis RIN4 is a target of the type III virulence effector AvrRpt2 and modulates RPS2-mediated resistance. *Cell* 112:379–389.
50. Cao H, Glazebrook J, Clarke JD, Volko S, Dong X (1997) The Arabidopsis NPR1 gene that controls systemic acquired resistance encodes a novel protein containing ankyrin repeats. *Cell* 88:57–63.
51. Yamada K, et al. (2011) Monosaccharide absorption activity of Arabidopsis roots depends on expression profiles of transporter genes under high salinity conditions. *J Biol Chem* 286:43577–43586.
52. von Malek B, van der Graaff E, Schneitz K, Keller B (2002) The Arabidopsis male-sterile mutant dde2-2 is defective in the ALLENE OXIDE SYNTHASE gene encoding one of the key enzymes of the jasmonic acid biosynthesis pathway. *Planta* 216:187–192.
53. Alonso JM, Hirayama T, Roman G, Nourizadeh S, Ecker JR (1999) EIN2, a bifunctional transducer of ethylene and stress responses in Arabidopsis. *Science* 284:2148–2152.
54. Jirage D, et al. (1999) Arabidopsis thaliana PAD4 encodes a lipase-like gene that is important for salicylic acid signaling. *Proc Natl Acad Sci USA* 96:13583–13588.
55. Wildermuth MC, Dewdney J, Wu G, Ausubel FM (2001) Isochorismate synthase is required to synthesize salicylic acid for plant defence. *Nature* 414:562–565.
56. Nishimura MT, et al. (2003) Loss of a callose synthase results in salicylic acid-dependent disease resistance. *Science* 301:969–972.
57. Whalen MC, Innes RW, Bent AF, Staskawicz BJ (1991) Identification of *Pseudomonas syringae* pathogens of *Arabidopsis* and a bacterial locus determining avirulence on both *Arabidopsis* and soybean. *Plant Cell* 3:49–59.
58. Hinsch M, Staskawicz B (1996) Identification of a new *Arabidopsis* disease resistance locus, *RPS4*, and cloning of the corresponding avirulence gene, *avrRps4*, from *Pseudomonas syringae* pv. *pisi*. *Mol Plant Microbe Interact* 9:55–61.
59. Martin M (2011) Cutadapt removes adapter sequences from high-throughput sequencing reads. *EMBnet J* 17:10–12.
60. Langmead B, Salzberg SL (2012) Fast gapped-read alignment with Bowtie 2. *Nat Methods* 9:357–359.
61. Kim D, et al. (2013) TopHat2: Accurate alignment of transcriptomes in the presence of insertions, deletions and gene fusions. *Genome Biol* 14:R36.
62. Anders S, Pyl PT, Huber W (2015) HTSeq–A Python framework to work with high-throughput sequencing data. *Bioinformatics* 31:166–169.
63. Robinson MD, McCarthy DJ, Smyth GK (2010) edgeR: A bioconductor package for differential expression analysis of digital gene expression data. *Bioinformatics* 26: 139–140.
64. Smyth GK (2005) limma: Linear models for microarray data. *Bioinformatics and Computational Biology Solutions Using R and Bioconductor* (Springer, New York), pp 397–420.
65. Storey JD, Tibshirani R (2003) Statistical significance for genomewide studies. *Proc Natl Acad Sci USA* 100:9440–9445.
66. de Hoon MJL, Imoto S, Nolan J, Miyano S (2004) Open source clustering software. *Bioinformatics* 20:1453–1454.
67. Eisen MB, Spellman PT, Brown PO, Botstein D (1998) Cluster analysis and display of genome-wide expression patterns. *Proc Natl Acad Sci USA* 95:14863–14868.
68. Love MI, Huber W, Anders S (2014) Moderated estimation of fold change and dispersion for RNA-seq data with DESeq2. *Genome Biol* 15:550.
69. Maere S, Heymans K, Kuiper M (2005) BiNGO: A cytoscape plugin to assess overrepresentation of gene ontology categories in biological networks. *Bioinformatics* 21: 3448–3449.
70. Rott M (2012) Structure *and Assembly Cues of* Arabidopsis *Root-Inhabiting Bacterial Communities and Comparative Genomics of Selected* Rhizobium *Members*. PhD dissertation (University of Cologne, Cologne, Germany).
71. Sasaki A, Yamaji N, Xia J, Ma JF (2011) OsYSL6 is involved in the detoxification of excess manganese in rice. *Plant Physiol* 157:1832–1840.